

# Pseudo Little Red Dot: an Active Black Hole Embedded in a Dense and Dusty, Metal-Poor Starburst Galaxy at $z = 5.96$

KARINA I. CAPUTI,<sup>1</sup> RYAN A. COOPER,<sup>1</sup> PIERLUIGI RINALDI,<sup>2</sup> RAFAEL NAVARRO-CARRERA,<sup>1</sup> AND EDOARDO IANI<sup>3</sup>

<sup>1</sup>*Kapteyn Astronomical Institute, University of Groningen, P.O. Box 800, 9700AV Groningen, The Netherlands*

<sup>2</sup>*Space Telescope Science Institute, 3700 San Martin Drive, Baltimore, MD 21218, USA*

<sup>3</sup>*Institute of Science and Technology Austria (ISTA), Am Campus 1, 3400 Klosterneuburg, Austria*

Submitted to ApJ

## ABSTRACT

We present a study of *Pseudo-LRD-NOM* (*Pseudo little red dot with no metal lines*), a highly magnified low-mass galaxy behind the lensing cluster Abell 370 at  $z = 5.96$ . We classify this object as a pseudo-LRD because its red rest-frame optical colour is mainly driven by a prominent  $\text{H}\alpha$  line (with  $\text{EW}_0 \gtrsim 800 \text{ \AA}$ ) present in its JWST NIRSpec spectrum.  $\text{H}\alpha$  is dominated by a narrow component and also has a minor broad component indicative of an active black hole with  $M_{\text{BH}} \approx 2.9 \times 10^6 M_{\odot}$ . A narrow  $\text{H}\beta$  emission line is also detected (with  $\text{S/N} = 8$ ), producing a Balmer decrement (narrow)  $\text{H}\alpha/\text{H}\beta = 11$ . The rest-frame UV spectral slope is  $\beta_{\text{UV}}^{\text{spec}} = -1.2$ . All these features can be ascribed to high dust attenuation. However, no  $[\text{OIII}]\lambda 5007$  or any other metal lines are detected in the spectrum, so  $[\text{OIII}]\lambda 5007/\text{H}\beta < 0.25$ , at odds with a simple dust-attenuation explanation. Accounting for all the spectral properties requires the model of a starburst with moderate colour excess  $E(\text{B-V})=0.18 - 0.45$ , high gas density ( $n_{\text{H}} \gtrsim 10^6 \text{ cm}^{-3}$ ) and extremely low gas/stellar metallicities ( $Z = 0.01 - 0.1 Z_{\odot}$ ). The demagnified stellar mass is  $1.62_{-0.79}^{+1.54} \times 10^7 M_{\odot}$  and the stellar-mass surface density is  $\Sigma_* = 418_{-310}^{+725} M_{\odot}/\text{pc}^2$ , similar to that of massive/nuclear star clusters. *Pseudo-LRD-NOM* provides evidence of massive black-hole growth occurring in a high-density, dusty starburst which is at the early stages of its chemical enrichment, and is likely a precursor to a real LRD.

**Keywords:** Active galaxies (17); Emission line galaxies (459); Galaxy abundances (574); Galaxy spectroscopy (2171); High-redshift galaxies (734)

## 1. INTRODUCTION

Understanding the formation of the galaxies that we see in the Universe today requires tracing their building blocks in cosmic time. These smaller units carried the imprint of the first stellar populations formed in those galaxies, as well as of the initial steps of chemical enrichment (e.g., Lebouteiller et al. 2013). At the same time, they are supposed to be the sites where black holes formed and efficiently started to grow (Greene et al. 2020). Therefore, spectroscopic studies of low stellar-mass galaxies (with  $M_* < 10^9 M_{\odot}$ ) at high redshifts can provide the key to unveiling the very basis of galaxy evolution.

Corresponding author: Karina I. Caputi  
karina@astro.rug.nl

The spectral properties of low stellar-mass galaxies, commonly called *dwarf galaxies* due to their relatively small sizes, have been extensively studied at low redshifts (e.g., Östlin et al. 2001; Guseva et al. 2009; Pérez-Montero et al. 2013; Amorín et al. 2014; Yang et al. 2017). They are typically characterised by prominent emission lines, indicative of high ionization states at sub-solar metallicities. In the rare cases that the metallicity is very low (e.g., Izotov et al. 2024), the metal lines are weak or absent, resembling the conditions that are expected to have been more common at early cosmic times.

However, until recently, spectroscopic observations of low-mass galaxies at high  $z$  were very challenging for existing telescopes, and thus only a handful of cases behind lensing fields could be studied (e.g., Vanzella et al. 2016; Karman et al. 2017; Vanzella et al. 2021). Thanks to the advent of JWST (Gardner et al. 2023), the study

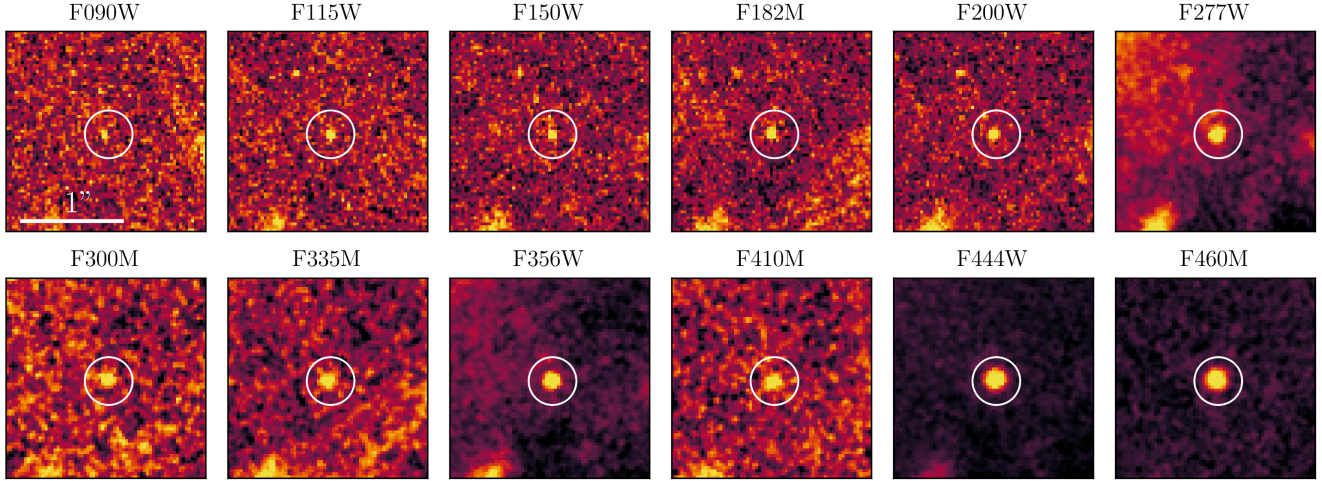


**Figure 1.** Postage stamps of *Pseudo-LRD-NOM* in different JWST/NIRCam bands. The two reddest filters shown, i.e., F444W and F460M, encompass the bright H $\alpha$  line.

of low-mass galaxies up to the Epoch of Reionization has now become routinely possible even in non-lensed fields (e.g., Schaefer et al. 2022; Castellano et al. 2024; Endsley et al. 2024; Harshan et al. 2024; Iani et al. 2024; Rinaldi et al. 2025a; Trussler et al. 2025).

In parallel, another high- $z$  galaxy population whose study has boomed in the JWST era is that of the so-called Little Red Dots (e.g., Kokorev et al. 2024; Matthee et al. 2024). These sources are characterised by being very compact (e.g., Baggen et al. 2024) and having a V-shaped  $f_{\lambda}(\lambda)$  spectral energy distribution (SED; e.g., Kocevski et al. 2025). Virtually all of them appear to harbour broad-line active galactic nuclei (BLAGN; e.g., Greene et al. 2024; Hvding et al. 2025). Based on the Balmer-line broadening, the central black holes appear to be overmassive with respect to their host galaxies (e.g., Harikane et al. 2023; Maiolino et al. 2024), in relation to what is expected from the local  $M_{\text{BH}} - M_{*}$  relation (Magorrian et al. 1998; Reines & Volonteri 2015). In addition, LRDs can show complex morphologies in the rest-frame UV, in spite of their compactness (e.g., Rinaldi et al. 2025b).

By selection most LRDs lie at  $z > 4$  and are typically hosted by low-mass galaxies, which sometimes are not even detected (e.g., Chen et al. 2025). Nonetheless, their metallicities do not stand out for being lower than average at high  $z$ , with the exception of a few known cases with  $Z \sim 0.1 Z_{\odot}$  (Taylor et al. 2025; Tripodi et al. 2025), including QSO1 behind the lensing cluster Abell 2744 (Furtak et al. 2023; D'Eugenio et al. 2025a; Maiolino et al. 2025a). This is also the case for other kinds of AGN at high redshifts, whose hosts are rarely metal poor (e.g., Matsuoka et al. 2018; Mignoli et al. 2019; Übler et al. 2023).

In LRD studies, galaxies with prominent emission lines driving the V-shaped SED colours are typically excluded (e.g., Kocevski et al. 2025). This is because the main goal is to select sources with a steeply rising rest-frame optical continuum which, in combination with the compactness criterion, allows for the identification of AGN candidates. We will argue that those discarded objects, which hereafter we call *pseudo-LRDs*, may merit attention on their own, as some of them could also contain AGN that are normally not accounted for in AGN demographic studies.

In this paper we present the analysis of a highly magnified low-mass galaxy, found behind the lensing cluster A370 at  $z = 5.96$ , which we name *Pseudo-LRD-NOM* (for *pseudo-LRD with no metal lines*) hereafter. This source stands out for having a rather unusual spectrum: it is characterised by the presence of a very prominent H $\alpha$  emission line, a much fainter but still significantly detected H $\beta$  line, but no [OIII] $\lambda 5007$  or any other metal lines. In addition, the rest-frame UV spectral slope  $\beta_{\text{UV}}^{\text{spec}}$  is quite high, which is indicative of significant dust attenuation.

The paper is organized as follows. In §2 we describe the utilised datasets, while in §3 we justify the motivation for the pseudo-LRD classification of our object. In §4 we present the spectroscopic and photometric properties of *Pseudo-LRD-NOM*, and investigate under which physical conditions all those properties can simultaneously be explained. In §5 we discuss our findings and compare some main properties of *Pseudo-LRD-NOM* and real LRDs. Finally, in §6 we present some concluding remarks. Throughout this paper, we consider a cosmology with  $H_0 = 70 \text{ km s}^{-1} \text{ Mpc}^{-1}$ ,  $\Omega_M = 0.3$ , and

$\Omega_\Lambda = 0.7$ , and a Chabrier (2003) initial mass function (IMF).

## 2. DATASETS

### 2.1. The lensing cluster A370

The source analysed here is gravitationally lensed by the massive galaxy cluster Abell370 (A370) at  $z = 0.375$ . This cluster is one out of the six targets included in the Hubble Space Telescope (HST) Frontier Fields program (Lotz et al. 2017; Bradač et al. 2019). Its background sources have been spectroscopically followed up from the ground in the pre-JWST era (e.g., Richard et al. 2021). With JWST, A370 and its background have been observed in a number of programs, including the Cycle 1 GTO CANUCS (P.I.: C. Willott, PID #1208); Cycle 2 GO program MAGNIF (P.I.: F. Sun; PID #2883); and program PID #3538 (P.I.: E. Iani).

The increasing data availability has allowed for a continuous improvement of the A370 lensing model. The latest versions, which incorporate JWST data, are those by Gledhill et al. (2024) and Diego et al. (2025). For our source we adopt here the magnification value provided in the CANUCS data release, i.e.  $\mu = 21.7 \pm 11.9$ .

### 2.2. JWST Spectroscopy

We analysed the source JWST spectrum taken with the Near Infrared Spectrograph's Micro-Shutter Array (NIRSpec/MSA; Ferruit et al. 2022) as part of the JWST Cycle 1 GTO program CANUCS (P.I.: C. Willott, PID #1208). This spectrum covers the wavelength range  $0.65.3 \mu\text{m}$  and has been obtained with the NIRSpec low-dispersion PRISM ( $R = 3030$ ). The spectrum was retrieved from the DAWN JWST Archive (DJA) and detailed data reduction steps can be found in Sarrouh et al. (2026).

### 2.3. Photometric Data

We retrieved and reprocessed all the NIRCam imaging available for A370. This includes imaging from the JWST programs CANUCS (P.I.: C. Willott, PID #1208); MAGNIF (P.I.: F. Sun; PID #2883); JUMPS (P.I. C. Withers; PID #5890); VENUS (P.I. S. Fujimoto; PID #6882); and programs PID #3538 (P.I.: E. Iani) and PID #5324 (P.I.: J. Pierel). For the data reduction, we employed our own custom NIRCam pipeline, which has already been tested and successfully applied in other JWST studies, including Rinaldi et al. (2023), Navarro-Carrera et al. (2024), Iani et al. (2024), and Caputi et al. (2024). Our software is based on the JWST pipeline version 1.20.2 (Bushouse et al. 2023), with the Calibration Reference Data System (CRDS) pipeline mapping (pmap) version 1471. It also includes

extra steps similar to those described by Bagley et al. (2023), including corrections for  $1/f$  noise, stray-light effects (wisps), and residual cosmic rays (snowballs).

As our source is compact, we measured  $0''.3$ -diameter aperture photometry and applied aperture corrections. We validated our photometry for *Pseudo-LRD-NOM* against the photometry provided in the publicly available CANUCS photometric catalog (Data Release 1; see Sarrouh et al. 2026), for the common passbands. We also considered the available HST photometry in this catalogue, corresponding to images that have been obtained from the HST CLASH and Frontier Fields programs (Postman et al. 2012; Lotz et al. 2017). We note that the choice of aperture, between  $0''.3$  and  $0''.7$ -diameter (corrected to total), and Kron apertures, does not affect the outcome of our spectral energy distribution (SED) fitting analysis (§4.3).

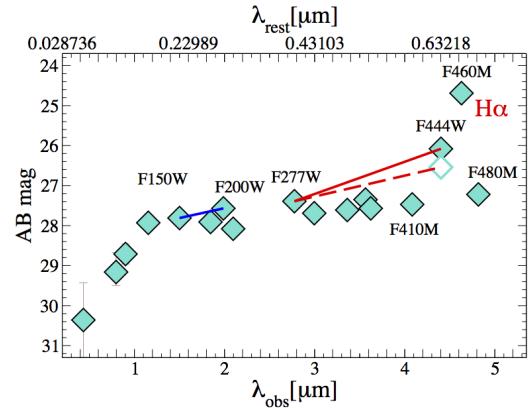


**Figure 2.** Observed photometry of *Pseudo-LRD-NOM*, uncorrected for magnification. For the F444W passband we show two data points, one corresponding to the original photometry (filled diamond) and another one obtained after correcting for the (minimum) flux density excess produced by the prominent  $\text{H}\alpha$  emission line over the continuum (empty diamond). The lines join the datapoints at the passbands that are typically used to define the LRD colour selection at  $z \sim 6$ : F115W-F200W (blue) and F277W-F444W (red solid and dashed for the original and  $\text{H}\alpha$ -corrected F444W photometry, respectively).

## 3. THE SOURCE PSEUDO-LRD-NOM

Our target source appears red and compact in the JWST NIRCam images (Fig. 1). Its red colour is boosted by the presence of a prominent  $\text{H}\alpha$  line, which we analyse in §4. If we subtract from the F444W photometry the flux density excess produced by  $\text{H}\alpha$  over the continuum, we see that the source could still have a red colour, as we show in Fig. 2. We computed the corrected F444W photometry by adding 0.46 mag to the

**Table 1.** Coordinates and main spectral line measurements for *Pseudo-LRD-NOM*.

Name	R.A. (J2000)	Dec. (J2000)	$z_{\text{spec.}}$	$f(\text{narrow H}\alpha)^a$	$f(\text{broad H}\alpha)^a$	$f(\text{H}\beta)^{a,b}$	$f([\text{OIII}]\lambda 5007)^a$
Pseudo-LRD-NOM	02:39:56.12	-01:34:25.19	5.96	$1017.6^{+56.0}_{-47.3}$	$394.6^{+42.4}_{-39.7}$	$92.5^{+11.4}_{-10.1}$	< 23.2

NOTE—a. Line fluxes are given in units of  $10^{-20} \text{ erg cm}^{-2} \text{s}^{-1}$  and are not corrected for magnification; b. A single narrow component is fitted to the  $\text{H}\beta$  line profile. The expected broad component is below the noise level (Fig. 4).

originally measured magnitude. This minimum correction corresponds to the lower limit of the total  $\text{H}\alpha$  rest-frame  $\text{EW}_0 \gtrsim 800 \text{ \AA}$  derived from the NIRSpec PRISM spectrum (see §4 and Fig. 3), as obtained using the formula provided by Mármlor-Queraltó et al. (2016).

The measured colours are:  $\text{F150W-F200W} = 0.24 \pm 0.09$  and  $\text{F277W-F444W} = 1.31 \pm 0.07$  (before correction for  $\text{H}\alpha$ ), changing to  $\text{F277W-F444W} \lesssim 0.85$  (after correction for  $\text{H}\alpha$ ). So, formally, the source is classified as an LRD if no  $\text{H}\alpha$  flux-density excess correction is applied. Once the correction is introduced, the resulting upper limit to the ( $\text{F277W-F444W}$ ) colour does not satisfy the LRD-selection criterion proposed by Kocevski et al. (2025), while it still satisfies the less strict criterion proposed by Kokorev et al. (2024).

Given the fact that the prominent  $\text{H}\alpha$  emission line is the main driver of the red ( $\text{F277W-F444W}$ ) colour of our source, we adopt the term ‘pseudo-LRD’ for it. Nonetheless, we highlight that, independently of the formal definition, the important point is that our source is very compact and harbours a BLAGN, as LRDs do.

In addition, the large photometric differences observed between the F410M and F460M filters, and then F460M and F480M, suggest that  $\text{EW}_0(\text{H}\alpha)$  is likely much larger than what is inferred from the spectral lower limit previously discussed. Applying the same formula quoted above from Mármlor-Queraltó et al. (2016), we derive that the  $\text{H}\alpha$  total  $\text{EW}_0$  could be as large as  $\text{EW}_0(\text{H}\alpha) \approx 3500 \text{ \AA}$ . This would imply that *Pseudo-LRD-NOM* is dominated by very young stellar populations (Prieto-Jiménez et al. 2025).

We present a complete SED analysis of *Pseudo-LRD-NOM* in §4.3 and provide its coordinates in Table 1.

#### 4. SPECTRAL AND PHOTOMETRIC ANALYSIS OF *PSEUDO-LRD-NOM*

##### 4.1. *Balmer line profiles*

Figure 3 shows the NIRSpec PRISM spectrum of our target. The Balmer  $\text{H}\alpha$  and  $\text{H}\beta$  emission lines are clearly visible, while no other lines are detected. The integrated  $\text{H}\alpha$  line has  $\text{S/N} > 25$ , while  $\text{S/N}(\text{H}\beta) \approx 8$ . Given this, the lack of  $[\text{OIII}]\lambda 5007$  emission is immediately striking.

We fitted the profiles of the  $\text{H}\alpha$  and  $\text{H}\beta$  lines using a two-Gaussian component model in each case. To correct for the line spread function, we used the `msafit` tool developed by de Graaff et al. (2024), which takes into account the position of the object in the NIRSpec slit, as well as the source morphology. Our results indicate that the  $\text{H}\alpha$  line has two components, a main narrow one and another fainter and broad (Fig. 4). The line profile fitting with two Gaussian components is significantly better than the one obtained with only one Gaussian or a Lorentzian profile. We applied a Bayesian information criterion (BIC; Schwarz 1978; Ronayne et al. 2025) to validate this result. The difference in the Bayesian index  $\Delta\text{BIC}$  that we have obtained is  $> 25$ , in favour of the two-Gaussian line profile model.

Instead, the  $\text{H}\beta$  line is fitted solely with a narrow component, while the expected broad component lies below the noise level. All our measured line fluxes are given in Table 1.

For the broad component of the  $\text{H}\alpha$  line we measured a full width at half maximum (FWHM) of  $4457^{+1406}_{-852} \text{ km s}^{-1}$ . This large broadening indicates the presence of an active black hole at the centre of our source, as is the case for basically all LRDs (e.g., Hviding et al. 2025). Note that a symmetric broadening of an emission line can be due to other factors, particularly clump rotation (e.g., Cooper et al. 2025). However, the large value of the line broad-component FWHM makes the clump-rotation hypothesis unlikely and, crucially, no clumps are visible in the high spatial resolution NIR-Cam images of *Pseudo-LRD-NOM*. We can also discard that the line broadening is produced by effects related to stellar kinematics, because such broadenings are typically much smaller than the value measured here for *Pseudo-LRD-NOM*’s  $\text{H}\alpha$  emission line (e.g., Tenorio-Tagle et al. 2010; Amorín et al. 2024).

Based on the broad  $\text{H}\alpha$ -line component, we can obtain an estimate of the central black-hole mass, following the prescription by Greene & Ho (2005). Considering the line FWHM and magnification-corrected flux, we get  $M_{\text{BH}} = 2.9^{+2.8}_{-1.3} \times 10^6 \text{ M}_{\odot}$ . This means that *Pseudo-LRD-NOM* hosts a massive black hole, but amongst

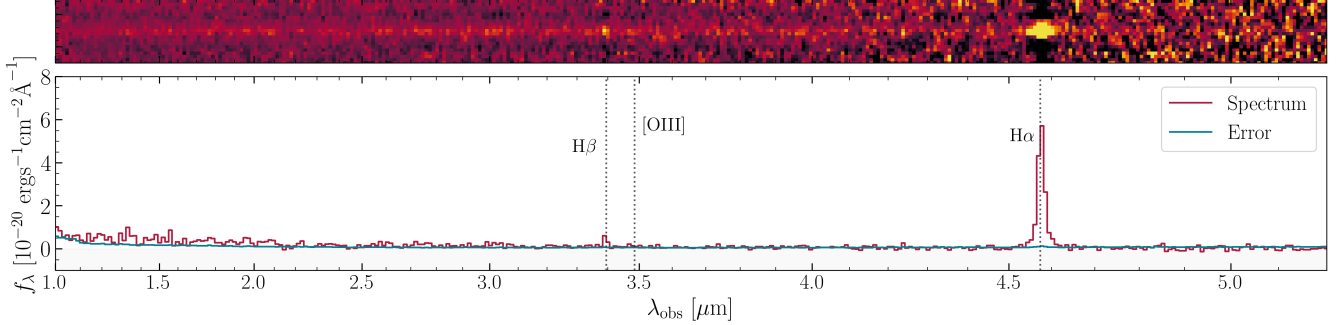


**Figure 3.** NIRSpec PRISM spectrum of *Pseudo-LRD-NOM*. While  $\text{H}\alpha$  and  $\text{H}\beta$  are clearly visible, no other emission lines are detected.

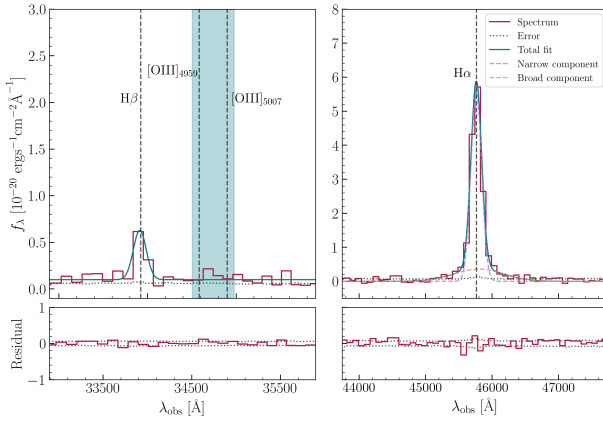


**Figure 4.** Zoomed-in views of the  $\text{H}\beta$  and  $\text{H}\alpha$  spectral lines (left and right panels, respectively). While a narrow and a broad component are clearly detected for  $\text{H}\alpha$ , only a narrow component is fitted for  $\text{H}\beta$ , with the expected broad component lying below the noise level.

the smallest typically found in LRDs at these redshifts, which can reach up to  $\sim 10^9 \text{ M}_\odot$  (e.g., Maiolino et al. 2025b; Taylor et al. 2025).

In turn, the flux measured on the narrow component of  $\text{H}\alpha$  can be used to obtain an estimate of the ongoing star formation rate (SFR) in the galaxy, under the assumption that existing calibrations to obtain SFRs from  $L(\text{H}\alpha)$  for high- $z$  galaxies are applicable to *Pseudo-LRD-NOM*. As we will show in §4.3, the minimum colour excess on the stellar models that can satisfactorily explain the spectral continuum of this source is  $E(B - V) \approx 0.18$ . Assuming the dust attenuation law by Calzetti et al. (2000), which is adequate for high- $z$  star-forming galaxies (McLure et al. 2018), we find that the magnification- and dust-corrected  $L(\text{narrow H}\alpha) \gtrsim (3.3 \pm 1.8) \times 10^{41} \text{ erg s}^{-1}$ . To convert this minimum  $\text{H}\alpha$  luminosity into an SFR, we considered the formula provided by Shapley et al. (2023) which is valid for low metallicities. We obtain  $\text{SFR}(\text{H}\alpha) \gtrsim (0.71 \pm 0.38) \text{ M}_\odot \text{ yr}^{-1}$ , which is very similar to the value obtained if we consider the conver-

sion formula provided by Theios et al. (2019) instead:  $\text{SFR}(\text{H}\alpha) \gtrsim (0.76 \pm 0.41) \text{ M}_\odot \text{ yr}^{-1}$ . This SFR implies that *Pseudo-LRD-NOM* is a starburst galaxy (see §4.3).

#### 4.2. Line ratios and their implications

##### 4.2.1. Interpretation of the line ratios

The measured fluxes for the narrow component of  $\text{H}\alpha$  and the total  $\text{H}\beta$  imply a Balmer decrement  $\text{H}\alpha/\text{H}\beta = 11.0^{+2.0}_{-1.7}$ , which is substantially higher than the value expected for a typical warm gas cloud with no dust following case B recombination (Osterbrock & Ferland 2006). High values of the  $\text{H}\alpha/\text{H}\beta$  ratio are commonly found amongst LRDs (e.g., de Graaff et al. 2025; D'Eugenio et al. 2025b; Furtak et al. 2025; Nikopoulos et al. 2025). A priori, such a high Balmer decrement is expected to be associated with a high dust attenuation of the warm gas. If we assume, for example, the dust reddening law by Calzetti et al. (2000), we obtain that the corresponding colour excess is  $E(B - V) \approx 0.88$ . Note that here the choice of reddening law is incidental: none of our main results or conclusions significantly depend on the considered prescription.

However, simply invoking dust attenuation is not sufficient to explain why no metal lines are detected in the spectrum of *Pseudo-LRD-NOM*. While dust attenuation could explain most of these non-detections, the lack of  $[\text{OIII}]\lambda 5007$  in particular is the key to infer that the situation is more complex. If the presence of dust attenuation were the only cause of  $[\text{OIII}]$  being undetected in the spectrum, then under standard conditions  $\text{H}\beta$  should be undetected as well. In the following we analyse plausible solutions to this problem.

Before any further analysis, though, there is a possible caveat to be considered. It could be that the flux of the  $\text{H}\beta$  line as it is observed comes partly or totally from the broad-line region, but appears as having only a narrow component because all flux beyond a central narrow window around the line center lies below the noise level. These considerations could change the narrow  $\text{H}\alpha/\text{H}\beta$

values quoted above. However, while at least a part of the  $H\beta$  flux comes from the host galaxy (or a narrow-line region), the problem remains the same: the lack of  $[\text{OIII}]\lambda 5007$  emission in the galaxy spectrum is a priori difficult to be reconciled with a simple dust-attenuation explanation.

Instead, if all the observed  $H\beta$  flux were part of the broad-line component and there is no flux associated with the narrow component of  $H\beta$ , then the lack of  $[\text{OIII}]\lambda 5007$  detection would not be puzzling, but rather a simple consequence of dust attenuation. To investigate if this could be the case, we performed a set of Monte Carlo simulations, as follows: we considered the broad component of  $H\alpha$  and renormalized it such that its peak flux density value coincided with the  $H\beta$  flux density peak. We also rebinned the profile to account for the different spectral resolutions of the NIR-Spec PRISM at the  $H\alpha$  and  $H\beta$  observed wavelengths. Then we made 1000 mock realizations of the  $H\alpha$  broad line component by assigning to each spectral element a random flux density value obtained from a Gaussian distribution centred at the real (renormalized) flux density, with an r.m.s. given by the noise level in the  $H\beta$  spectral window. For each resulting mock broad line we measured the FWHM. Our results are presented in Fig. 5. The obtained distribution of FWHM for the simulated broad line components has a median/r.m.s.  $\text{FWHM}(H\alpha) = (4776.5 \pm 246.4) \text{ km s}^{-1}$ , which is consistent within the errors with the FWHM of the original  $H\alpha$  broad component ( $4457^{+1406}_{-852} \text{ km s}^{-1}$ ). The measured  $\text{FWHM}(H\beta)$  is  $> 10\sigma$  away. Therefore, we conclude that the observed  $H\beta$  line is genuinely dominated by the narrow component. In all the following we will then consider that  $f(H\beta) = f(\text{narrow } H\beta)$ .

#### 4.2.2. The $H\alpha/H\beta$ vs. $[\text{OIII}]\lambda 5007/H\beta$ diagram

In Fig. 6 we show the (narrow)  $H\alpha/H\beta$  versus  $[\text{OIII}]\lambda 5007/H\beta$  ratios for our source. For context we also plot the ratios corresponding to a general sample of low-mass galaxies at  $z > 4$  (Cooper et al., in prep.) and a few LRDs from the literature (Furtak et al. 2023; Greene et al. 2024; D’Eugenio et al. 2025a; Maiolino et al. 2025a). From this figure we can see that the vast majority of low-mass galaxies follow a broad correlation in this diagram, as it is expected from the canonical situation in which the oxygen abundance (which is one of the main parameters governing the  $[\text{OIII}]/H\beta$  ratio) increases with dust attenuation, as given by the  $H\alpha/H\beta$  ratio. Instead, some LRDs appear to be off this relation. This is particularly evident for our source *Pseudo-LRD-NOM*, which strongly suggests that the physical conditions are different in these objects.

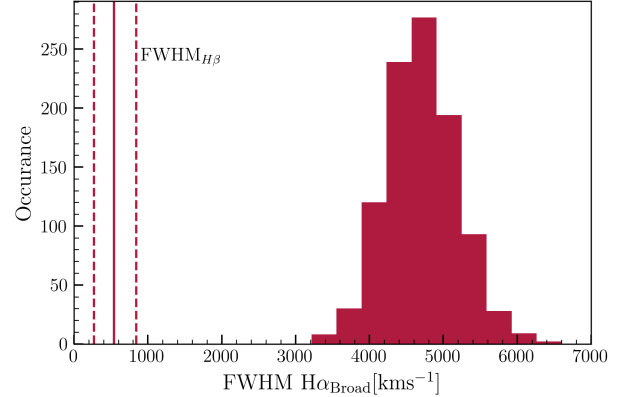


**Figure 5.** FWHM distribution for 1000 mock realizations of the broad  $H\alpha$  line obtained after renormalizing its peak to the peak flux of  $H\beta$  and degrading its S/N ratio to that observed in the  $H\beta$  spectral window. In all cases these FWHM are much larger than that observed for  $H\beta$ . This means that  $H\beta$  is genuinely dominated by a narrow component.

The upper limit on the  $[\text{OIII}]/H\beta$  ratio ( $< 0.25$ ) can be used to obtain an estimate of the upper limit of the gas metallicity  $12 + \log_{10}(\text{O/H})$ . Although in principle the relation between these two quantities is bivariate, the upper metallicity branch can safely be discarded by the lack of metal lines in the spectrum. Considering the recent calibration obtained by Cataldi et al. (2025), for *Pseudo-LRD-NOM* we obtain  $12 + \log_{10}(\text{O/H}) < 7.0$ , i.e.  $< 0.02 Z_\odot$  (this value would be even lower considering other calibrations from the literature). So this would suggest that the ISM warm gas in *Pseudo-LRD-NOM*’s host is close to pristine condition. However, these calibrations are based on galaxies whose ISM’s densities are less extreme than for *Pseudo-LRD-NOM*, so their application to LRDs may not be straightforward, as we discuss below.

We produced a range of line emission models using the software CLOUDY (Ferland et al. 2013, 2017) to investigate under which conditions the observed line ratios of *Pseudo-LRD-NOM* can be reproduced. For our ionizing source, we consider stellar population models from BPASS (Eldridge et al. 2017) that include a burst in star formation and binary systems. We consider both solar and sub-solar metallicities for the stellar and gas-phase metallicities and employ stellar populations with ages in the range  $10^6$  to  $10^8$  years. These stars are the only source of ionizing photons in our model and no dust is present in any of our models.

Although we will argue in §4.3 that *Pseudo-LRD-NOM* actually has non-negligible dust attenuation of its spectral continuum, the main objective here is to show that the spectral line ratios can be explained even without invoking the presence of dust. We will discuss later

the implications of the high Balmer decrements being partly produced by dust attenuation (see §4.3).

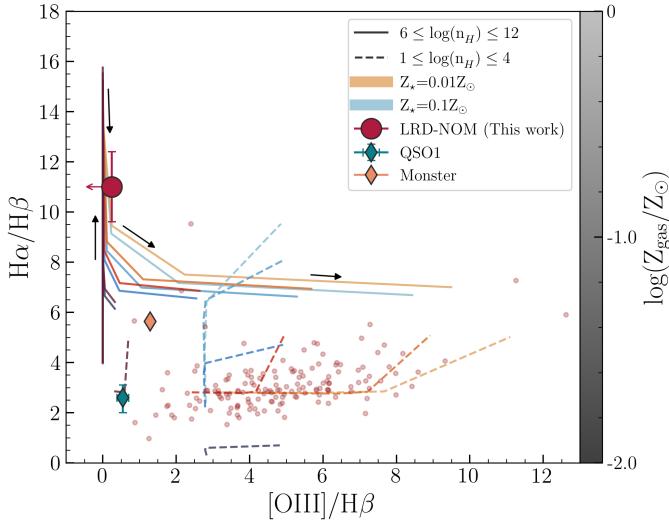


**Figure 6.** Balmer decrement  $H\alpha/H\beta$  versus  $[\text{OIII}]\lambda 5007/H\beta$  for our source *Pseudo-LRD-NOM* (red filled circle) and LRDs from the literature: the Monster (orange diamond; Greene et al. 2024; Labb   et al. 2025) and QSO1 (teal diamond; Furtak et al. 2025; D'Eugenio et al. 2025a; Maiolino et al. 2025a), both behind Abell 2744. The small orange circles represent a general sample of low stellar-mass ( $M_* < 10^9 M_\odot$ ) galaxies at  $z > 4$  (Cooper et al., in prep.). The solid lines show the line ratios predicted by CLOUDY models for a starburst with age 1 Myr, and a range of gas and stellar metallicities, as indicated in the intensity bar and inset label. The tracks move along the gas volume density values  $n_H$ , in the range specified in the inset label.

In Fig. 6 we show the CLOUDY model tracks corresponding to a very young starburst with age 1 Myr. We see that only models with high gas density ( $n_H > 10^6 \text{ cm}^{-3}$ ) can reproduce *Pseudo-LRD-NOM*'s line ratios. Stellar and gas metallicities between  $0.01 Z_\odot$  and  $0.1 Z_\odot$  are all similarly suitable. Note that the high gas densities needed for our source are above the  $[\text{OIII}]\lambda 5007$  critical density, which is  $7 \times 10^5 \text{ cm}^{-3}$  (Osterbrock & Ferland 2006; Baskin & Laor 2005). This means that, in *Pseudo-LRD-NOM*, the  $[\text{OIII}]\lambda 5007$  line emission would mainly be governed by collisional excitation rather than photoionization.

Therefore, the extremely low metallicities inferred from calibrations based on more normal galaxies should be taken with caution in this case, as very high gas densities can also be a driver of low  $[\text{OIII}]/H\beta$  ratios. Deeper spectroscopic data allowing for a stronger constraint on the  $[\text{OIII}]\lambda 5007$  emission is necessary to conclude on extremely low metallicities for *Pseudo-LRD-NOM*.

The physical conditions derived for *Pseudo-LRD-NOM* are in contrast with those for the vast majority of low-mass galaxies, whose line ratios can be reproduced by models of starbursts with much lower gas densities (Fig. 6). At the same time, the line ratios of QSO1 can also be reproduced with models of starbursts with moderate densities, but only in combination with very low gas/stellar metallicities.

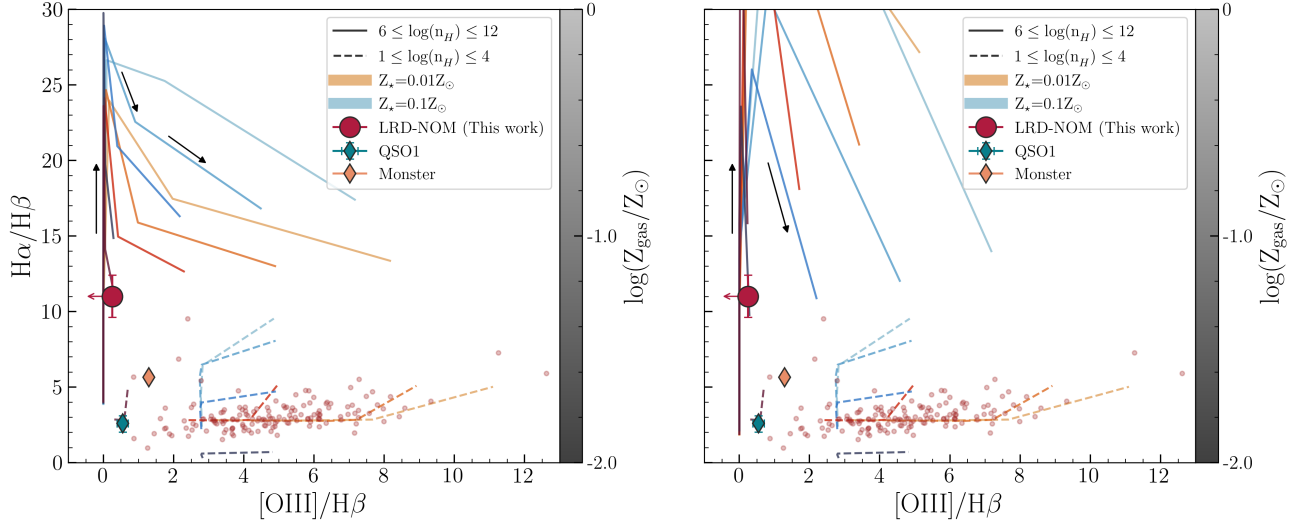
Crucially, the CLOUDY models considered here do not incorporate any dust attenuation, which indicates that the physical conditions of the host in which *Pseudo-LRD-NOM* is embedded can be explained without invoking any dust. The very high densities and low metallicities which are necessary to reproduce the spectral lines of *Pseudo-LRD-NOM* are similar to those of nuclear star clusters or proto-globular clusters (e.g., Vanzella et al. 2023; Adamo et al. 2024). We note that recently Yan et al. (2025) also analysed the physical conditions to explain the high Balmer decrements observed in some LRDs without the need of dust. However, these models were based on the assumption that the main radiation source is the central AGN, while here we only consider stellar emission to model *Pseudo-LRD-NOM*.

Fig. 7 is equivalent to Fig. 6, but shows CLOUDY model tracks corresponding to older starbursts with ages 10 and 100 Myr. We see that in these two cases we can also reproduce the spectral line ratios of *Pseudo-LRD-NOM* with the models of dust-free very dense starbursts. However, interestingly, as the age increases, only very low gas-metallicity models are suitable.

#### 4.3. Further clues from the spectral slope $\beta_{\text{UV}}^{\text{spec}}$ and SED fitting on the photometry

To further understand *Pseudo-LRD-NOM*'s nature, we study its SED as traced by the HST and NIRCam broad-band photometry. For the SED fitting, we did not incorporate the F460M filter photometry, though, as it is significantly affected by the  $H\alpha$  emission.

We made use of the SED-fitting code CIGALE (Boquien et al. 2019), considering different combinations of stellar+nebular and stellar+AGN models. For the stellar templates we employed a delayed star-formation history with a secondary burst, allowing the age of the stellar population to select from 1 Myr to 1000 Myr. Stellar populations are produced from BC03 models (Bruzual & Charlot 2003), with stellar metallicities varying between  $Z_\odot$  and  $\sim 1/1000 Z_\odot$ . We included the effect of dust attenuation following a modified Calzetti et al. (2000) attenuation law with  $E(B-V)$  values ranging from 0 to 1. For the stellar+nebular model, nebular emission is included with a fixed ionization parameter  $\log_{10}(U) = -2$  and gas-phase metallicities varying



**Figure 7.** The same as Fig. 6, but showing CLOUDY model tracks for older starbursts with ages 10 Myr (left) and 100 Myr (right).

across the same range as the stellar metallicity. In the stellar+AGN model, we utilise the SKIRTOR 2016 AGN model (Stalevski et al. 2016) with an opening angle of  $70^\circ$  and AGN fractions of 0, 0.01, and 0.1 – 0.9 with steps of 0.1.

Fig. 8 shows the best-fit SEDs obtained using a combination of stellar and nebular templates, and a combination of stellar and AGN templates. We see that both combinations produce a good fit to the total SED, with the combination of stellar and AGN templates slightly preferred (although the derived AGN contribution to the SED is only  $\approx 10\%$ ). Both template combinations yield very similar stellar masses, indicating that the obtained stellar mass can be considered robust. Reassuringly, for any of the template combinations, the properties of the stellar component are quite similar: in both cases, the stellar metallicity is the lowest possible, the age is quite young ( $\approx 44$  – 124 Myr) and the colour excess is significant. Forcing CIGALE to consider only higher metallicity models and/or higher ages reduces the output  $E(B-V)$  value, but the resulting reduced  $\chi^2$  is significantly higher, indicating that these alternative solutions are not preferred.

We investigated whether this need for dust attenuation for the stellar continuum could be related to the special conditions revealed by the spectral properties of *Pseudo-LRD-NOM*. To do this we compared the rest-frame UV continuum slope  $\beta_{UV}$  derived from CIGALE’s best-fit stellar models with those produced by CLOUDY for the models that best reproduce the spectral line ratios (Fig. 6 and 7). For all these models, the intrinsic  $\beta_{UV}$  values are very small ( $\beta_{UV} < -2$ ). A non-negligible amount of dust attenuation is necessary to reproduce the

relatively red  $\beta_{UV}^{\text{spec}} = -1.2$  measured on *Pseudo-LRD-NOM*’s spectrum.

For the case of a 1 Myr old starburst, there are multiple CLOUDY tracks that reproduce our *Pseudo-LRD-NOM*’s spectral line ratios. They all have  $\beta_{UV}$  values between -2.8 and -2.9, which implies that a colour excess  $E(B-V) = 0.34$  – 0.36 would be necessary to reproduce  $\beta_{UV}^{\text{spec}} = -1.2$  measured on *Pseudo-LRD-NOM*’s spectrum (assuming the Calzetti et al. (2000) dust-attenuation law; see e.g., Reddy et al. (2018)). For a 10 Myr old starburst, only models with very high gas density ( $n_H > 10^{10} \text{ cm}^{-3}$ ) and very low metallicities ( $Z \approx 0.01 Z_\odot$ ) can reproduce the observed line ratios. Such models have  $\beta_{UV} = -3.2$ , so a value  $E(B-V) = 0.43$  is required to flatten the rest-frame UV slope to the observed value. Finally, for the 100 Myr old starburst, the track that reproduces the line ratios has  $\beta_{UV} = -2.05$ , which implies the need of  $E(B-V) = 0.18$  to account for the observed  $\beta_{UV}^{\text{spec}} = -1.2$ .

In the light of these findings, it is likely that the  $H\alpha/H\beta$  line ratio is at least partly affected by dust attenuation. The colour excess values derived above imply that the effect of dust attenuation could by itself produce an  $H\alpha/H\beta$  ratio between  $\approx 3.8$  and 5.5. Considering that the gas could have up to  $\times 2$  higher attenuation than the stars (e.g., Reddy et al. 2020; Shvai et al. 2020), the resulting  $H\alpha/H\beta$  ratio could be between 7.6 and  $\approx 11.0$ . Only the latter value is as high as the observed  $H\alpha/H\beta$  ratio.

At the same time, one has to consider that the  $[OIII]/H\beta$  is virtually independent of dust attenuation. If the intrinsic (unattenuated)  $H\alpha/H\beta$  value were very low, then *Pseudo-LRD-NOM* would be located close

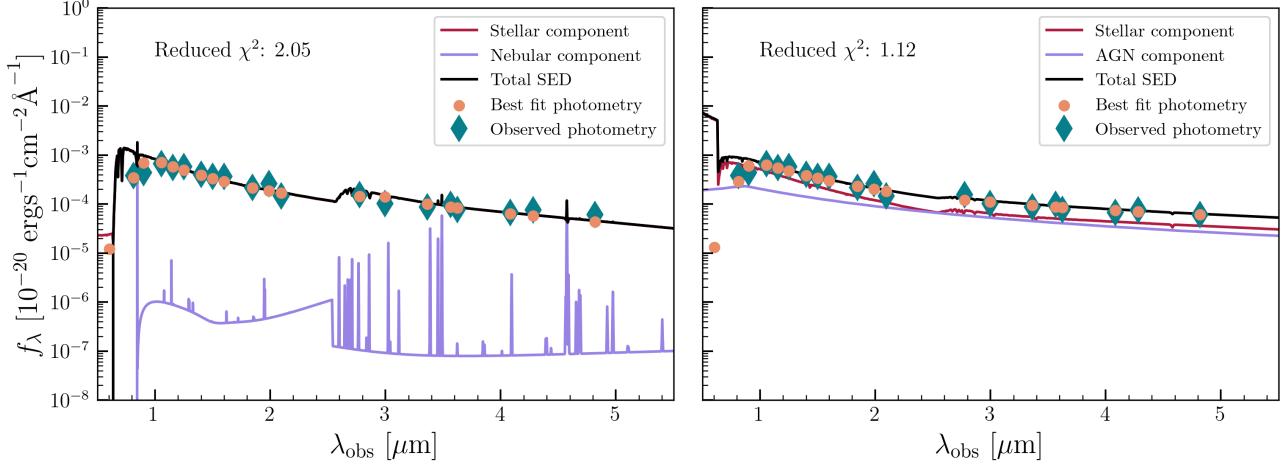


**Figure 8.** The best-fit SEDs obtained with CIGALE on the source NIRCam photometry, with different model combinations. *Left:* stellar template + nebular emission. The nebular emission contribution is virtually insignificant. *Right:* Stellar template + AGN. The AGN component makes for  $\approx 10\%$  of the total SED. The best fit parameters are given in Table 2.

to QSO1 in Fig. 6. The inferred gas densities would be lower, but also the necessary gas/stellar metallicities. And this would have to be coupled with high dust extinction to reproduce the observed line ratios for *Pseudo-LRD-NOM*, resulting in a more intriguing scenario, which we discuss in §5.

The stellar mass derived from the SED fitting is  $\log_{10}(M_*/M_\odot) = 8.55 \pm 0.20$ , which after correction for magnification becomes  $\log_{10}(M_*/M_\odot) = 7.21 \pm 0.29$  (considering  $\mu = 21.7 \pm 11.9$ ). Considering the dust- and magnification-corrected SFR lower-limit that we derived in §4.1, i.e.,  $\text{SFR}(\text{H}\alpha) \gtrsim 0.71 \pm 0.38 M_\odot \text{yr}^{-1}$ , we get a specific SFR value  $\log_{10}(\text{sSFR}/\text{yr}^{-1}) \gtrsim -7.36 \pm 0.32$  (which is independent of magnification). This high minimum sSFR implies that *Pseudo-LRD-NOM* is a starburst galaxy, following the empirical starburst definition of Caputi et al. (2017, 2021).

Finally, the estimated half-light radius of the source, as obtained from the F150W-band image, is  $(520 \pm 270)$  pc. After correction for magnification it becomes  $R_{1/2} = (112 \pm 80)$  pc. This gives a stellar-mass surface density  $\Sigma_* = 418^{+725}_{-310} M_\odot/\text{pc}^2$  (independent of magnification). This is similar to the stellar surface density found in massive star clusters (Vanzella et al. 2023; Mowla et al. 2024) and even compatible within the error bars with the stellar surface density of nuclear star clusters (e.g., Neumayer et al. 2020; Fahrion et al. 2021).

## 5. DISCUSSION

### 5.1. The complex scenario revealed by the simple spectrum of *Pseudo-LRD-NOM*

The spectral properties of *Pseudo-LRD-NOM* are quite unusual, as they include a high Balmer decrement (narrow)  $\text{H}\alpha/\text{H}\beta = 11.0$  simultaneously with a low ra-

**Table 2.** Best-fit SED parameters for *Pseudo-LRD-NOM*.

Parameter	Stellar + Nebular	Stellar + AGN
Reduced $\chi^2$	2.05	1.12
$\log_{10}(M/M_\odot)^a$	$8.68 \pm 0.72$	$8.55 \pm 0.20$
$E(\text{B}-\text{V})^b$	$0.33 \pm 0.20$	$0.45 \pm 0.17$
Age (Myr)	$124.2 \pm 95.3$	$44.5^{+44.5}_{-40.2}$
Stellar Metallicity	$0.0001 \approx 0.7\% Z_\odot^c$	$0.0001 \approx 0.7\% Z_\odot^c$

NOTE—Results at fixed  $z_{\text{spec}} = 5.96$ . a) The quoted stellar masses do not carry any magnification correction. b) The colour excess applies only to the stellar component. c) Considers that the solar metal fraction is  $Z_\odot = 0.014$  (Asplund et al. 2009).

tio  $[\text{OIII}]\lambda 5007/\text{H}\beta < 0.25$ . High Balmer decrements are relatively common amongst LRDs (e.g., Nikopoulos et al. 2025; Rusakov et al. 2025). Although some first studies have explained them simply by the presence of dust attenuation, the lack of mid-infrared emission of many LRDs (e.g., Prez-Gonzalez et al. 2024; Setton et al. 2025) suggests a more complicated picture. Very recently, Yan et al. (2025) showed that high Balmer decrements can be explained via high-density gas emission from the AGN broad-line region within the LRDs, without the need of invoking dust.

The situation for *Pseudo-LRD-NOM* is somewhat different, as the high  $\text{H}\alpha/\text{H}\beta$  is dominated by the narrow line components, which originate in the narrow-line region or the galaxy host (we have not made the difference between the two in this paper, as the available spectrum does not have the necessary spatial information for this purpose). We showed here that a very dense and young, metal-poor starburst can produce the observed line ra-

tios. Although invoking dust attenuation is in principle not necessary to explain the high  $H\alpha/H\beta$ , we do infer the presence of dust from the relatively flat rest-frame UV continuum slope  $\beta_{\text{UV}}^{\text{spec}} = -1.2$  derived from *Pseudo-LRD-NOM*'s spectrum.

Fig. 9 shows a comparison of the *Pseudo-LRD-NOM* and QSO1 spectra. A main difference between the two is the strength of the Balmer break, which is very evident for QSO1 (Ji et al. 2025), and absent for *Pseudo-LRD-NOM*. The prominent Balmer breaks observed in some LRDs do not have a stellar origin, but are rather produced by ultra-dense ( $n_H \gtrsim 10^{10} \text{ cm}^{-3}$ ) and turbulent gas, most likely present in the AGN broad-line region (e.g., Inayoshi & Maiolino 2025). This ultra-dense gas can trap the UV photons produced by the black-hole accretion, resulting in the sharp spectral drop observed at short wavelengths (e.g., Liu et al. 2025). The lack of such a sharp feature for *Pseudo-LRD-NOM* may be indicating that its central black hole is not surrounded by such ultra-dense gas structure. And the gas in its host galaxy, even if dense, does not reach the ultra-high densities of the gas in LRD's broad-line regions.

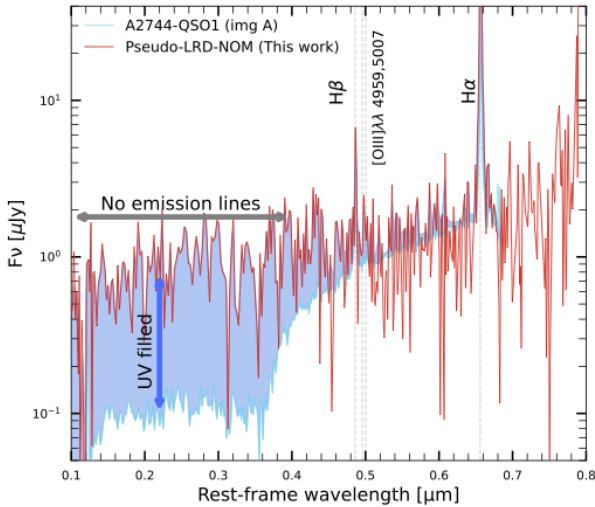


**Figure 9.** Comparison of the *Pseudo-LRD-NOM* and QSO1 spectra, renormalized at rest-frame wavelength  $\approx 0.53 \mu\text{m}$ .

The lack of a significant Balmer break makes *Pseudo-LRD-NOM* resemble other kinds of AGN found to be hosted by low-metallicity galaxies at high  $z$  (e.g., Übler et al. 2023). In all these sources, the flux of UV photons is high enough to make the Balmer break disappear.

### 5.2. An active black hole in a dense star cluster

Interestingly, almost all the light of *Pseudo-LRD-NOM* can be explained by having a stellar origin, with the need of only a minor AGN component for the SED.

The presence of an AGN becomes most evident by the identification of a broad component in the  $H\alpha$  line. Although a broad-line component could in principle have a different origin, its FWHM is so large that the association with an active black hole is the most likely explanation. The presence of a BLAGN is now recognised as quintessential to the LRD nature. However, the black-hole masses derived from the line broadening are systematically higher than what is expected from the local (and even high- $z$ )  $M_{\text{BH}}$  vs.  $M_*$  relation (e.g., Harikane et al. 2023; Pacucci et al. 2023). The situation for *Pseudo-LRD-NOM* is similar: we find  $M_{\text{BH}}/M_* \approx 0.18$ , which means that the central black hole is overmassive by 1-2 orders of magnitude. So the presence of overmassive black holes is not exclusive to LRDs, but rather also applies to other types of AGN at high  $z$  (e.g., Onoue et al. 2019; Harikane et al. 2023). Alternatively, it could be that the line broadening is enhanced by physical processes other than kinematics of the broad-line region, in which case the black-hole masses could be overestimated. For example, electron scattering in dense ionized gas clouds could be partly responsible for the line broadening (e.g., Laor 2006; Inayoshi & Ho 2025).

*Pseudo-LRD-NOM*'s host appears to be a dense and dusty starburst, with a stellar density typical of massive star clusters and even nuclear star clusters. The simultaneous presence of an AGN and a nuclear star cluster in LRDs has been recently proposed via theoretical considerations (e.g., Inayoshi et al. 2025). The spectral properties of *Pseudo-LRD-NOM* reveal that this combination is present in this source. As a matter of fact, the connection between nuclear star clusters and black-hole growth has been investigated since at least a few decades ago (e.g., Portegies Zwart et al. 2004, 2006).

In general, it is believed that the presence of nuclear star clusters could facilitate the efficient growth of massive black holes by funneling gas to the galaxy centre (e.g., Naiman et al. 2015; Partmann et al. 2025; Su et al. 2025). They could potentially explain the early growth of massive black holes via synchronised episodes of black-hole accretion and nuclear star formation. The identification and further study of other low-mass galaxies with nuclear activity and high stellar/gas densities are necessary to understand the details of this phenomenon.

Recently Dekel et al. (2025) proposed a mechanism for LRD formation: star clusters merging to form compact central star clusters. Each star cluster carries a core-collapse black hole, which contributes to the formation of a central, massive black hole in the merging process. A series of gas-rich compaction events deepen the galaxy central potential well, allowing for the reten-

tion of the central black hole. In this scenario, which is similar to that considered by Inayoshi et al. (2025), *Pseudo-LRD-NOM* could represent a system which is in between compaction events. The inflow of pristine gas from the dark matter halo could keep the metallicity low until the compaction triggers new star formation activity and subsequent chemical enrichment. So, in summary, *Pseudo-LRD-NOM* could constitute an LRD in the making.

We note that *Pseudo-LRD-NOM*'s nature is in principle different to that of the local *blueberry galaxies* studied by Yang et al. (2017) and the *little blue dots* studied by Elmegreen & Elmegreen (2017). These galaxy populations have low masses and are metal poor, but are also significantly less compact than *Pseudo-LRD-NOM*. Therefore, their resulting stellar mass surface densities are also lower. In addition, by selection these galaxies are dust-free and have no reported evidence of the presence of black-hole activity.

### 5.3. The simultaneous presence of extremely low metallicities and dust attenuation

Another property inferred for *Pseudo-LRD-NOM*'s host is its very low metallicity:  $Z = 0.01\text{--}0.1 Z_{\odot}$  for the gas and stars from the spectral modelling, and even lower stellar metallicities from the SED fitting. Sub-solar metallicities are the rule amongst low-mass galaxies at high  $z$ , and some LRD hosts have been found to have gas metallicities of  $\sim 0.1 Z_{\odot}$  (e.g., Maiolino et al. 2025a; Taylor et al. 2025; Tripodi et al. 2025). *Pseudo-LRD-NOM* appears to be at an earlier stage of chemical enrichment.

What is particularly remarkable for *Pseudo-LRD-NOM* is the simultaneous presence of very low metallicities and significant dust attenuation. The presence of dust in metal-poor galaxies is known at low  $z$  (e.g., Galliano et al. 2005; Rémy-Ruyer et al. 2013; Izotov et al. 2014). It has also been reported in metal-poor, star-forming galaxies at high  $z$ , particularly gamma-ray burst hosts (Heintz et al. 2023a). It can be explained via a quick dust injection produced by supernovae (e.g., Hirashita et al. 2002; Martínez-González et al. 2022) or carbon-enriched Wolf Rayet stars (Lau et al. 2021), before the galaxy becomes significantly metal-enriched. Early metal pollution from massive stars has recently been invoked to explain the metal abundances of higher  $z$  galaxies, such as GNz11 (Ebihara et al. 2026).

Thus, *Pseudo-LRD-NOM* could be at a more advanced chemical enrichment stage than sources dominated by pristine gas, but still be at the initial stages of chemical enrichment. Alternatively, the low metallicity could be maintained by a continuous accretion

of pristine gas from the dark matter halo in which *Pseudo-LRD-NOM* resides, producing metal dilution (e.g., Cresci et al. 2010; Troncoso et al. 2014; Heintz et al. 2023b). The search for signatures of inflowing gas in other sources showing metal lines in their spectra would help to test this scenario.

The results of the SED fitting suggest that *Pseudo-LRD-NOM*'s host is a young starburst with age 44–124 Myr. In turn, the flux density excess (with respect to the continuum) observed in the F460M filter due to the presence of  $\text{H}\alpha$  indicates that  $\text{EW}_0(\text{H}\alpha)$  could be as large as  $\sim 3500 \text{ \AA}$ . In this case, *Pseudo-LRD-NOM* could be dominated by even younger stellar populations of age  $\lesssim 1 \text{ Myr}$ .

A further intriguing possibility is that *Pseudo-LRD-NOM* could be hosting Population III (Pop III) stars. These stellar populations are in principle expected to have spectra with only emission lines produced by H and He atomic transitions (e.g., Nakajima & Maiolino 2022), but some minor metal self-pollution may be possible, even while PopIII stars still dominate the new star-forming regions (e.g., Sarmento et al. 2017; Rusta et al. 2025). To date, only a small amount of high- $z$  candidates have been found to likely host significant PopIII star-formation activity (e.g., Vanzella et al. 2023; Morishita et al. 2025).

The lack of  $\text{HeII}\lambda 4686$  emission in *Pseudo-LRD-NOM*'s spectrum prevents us to extract such a conclusion. We note that the spectral continuum is marginally detected at the position of the  $\text{HeII}\lambda 4686$  emission line and, thus, the line should also be detected if such emission were present, unless the dust attenuation on the gas is larger than in the stellar component. A wider investigation of sources like *Pseudo-LRD-NOM*, and dwarf galaxies in general at high  $z$ , is necessary to find sources with a significant presence of first stellar generations.

## 6. CONCLUSIONS

We presented a detailed study of *Pseudo-LRD-NOM*, a source at  $z = 5.96$  which would fail the LRD classification because of its red rest-frame optical colour being mainly driven by the presence of a prominent  $\text{H}\alpha$  line. We inferred the presence of an active, massive black hole in *Pseudo-LRD-NOM* by  $\text{H}\alpha$  having a very broad component, whose high FWHM cannot be explained by stellar kinematics. We argued that the study of pseudo-LRDs has so far been largely neglected in the literature, but it could still be important to obtain a complete AGN census at high redshifts.

Moreover, *Pseudo-LRD-NOM* provides evidence for an active black hole being embedded in a high-density, dusty starburst which is still at the early stages of its

chemical enrichment. *Pseudo-LRD-NOM* is likely the precursor to a real LRD, with the massive central black-hole already in place, but without yet having the ultradense cocoon that would produce a prominent Balmer break in its spectrum. The study of more pseudo-LRDs residing in low-mass galaxies could be a key route to investigate the connection between massive black-hole growth and nuclear star clusters, as well as the LRD formation mechanisms. In addition, integral field spectroscopic studies with medium/high spectral resolution, with JWST and future 30-40 m-class ground-based telescopes, will be necessary to reveal in detail the dynamics and other physical processes at play in these sources.

We thank Daniela Calzetti, Kohei Inayoshi, and Zu Yan for useful discussions.

This work is based on observations made with the NASA/ESA/CSA JWST. The data were obtained from the Mikulski Archive for Space Telescopes at the Space Telescope Science Institute, which is operated by the Association of Universities for Research in Astronomy, Inc.,

under NASA contract NAS 5-03127 for JWST. These observations are associated with the JWST GTO program PID 1208. Some of the data products presented in this paper were retrieved from the Dawn JWST Archive (DJA). DJA is an initiative of the Cosmic Dawn Center (DAWN), which is funded by the Danish National Research Foundation under grant DNRF140. Also based on observations made with the NASA/ESA Hubble Space Telescope obtained from the Space Telescope Science Institute, which is operated by the Association of Universities for Research in Astronomy, Inc., under NASA contract NAS 526555.

KIC and RNC acknowledge funding from the Dutch Research Council (NWO) through the award of the Vici Grant VI.C.212.036.

*Facilities:* JWST, HST.

*Software:* ASTROPY (Astropy Collaboration et al. 2022), CIGALE (Boquien et al. 2019), CLOUDY (Ferland et al. 2013, 2017), MSAEXP (Brammer 2023), NUMPY (Harris et al. 2020), PANDAS (team 2024), PHOTUTILS (Bradley et al. 2016), TOPCAT (Taylor 2022).

## REFERENCES

Adamo, A., Bradley, L. D., Vanzella, E., et al. 2024, *Nature*, 632, 513

Amorín, R., Sommariva, V., Castellano, M., et al. 2014, *A&A*, 568, L8

Amorín, R. O., Rodríguez-Henríquez, M., Fernández, V., et al. 2024, *A&A*, 682, L25

Asplund, M., Grevesse, N., Sauval, A. J., & Scott, P. 2009, *Annual Review of Astronomy and Astrophysics*, 47, 481

Astropy Collaboration, Price-Whelan, A. M., Lim, P. L., et al. 2022, *The Astrophysical Journal*, 935, 167A  
<https://ui.adsabs.harvard.edu/abs/2022ApJ...935..167A>

Baggen, J. F. W., van Dokkum, P., Brammer, G., et al. 2024, *ApJL*, 977, L13

Bagley, M. B., Finkelstein, S. L., Koekemoer, A. M., et al. 2023, *ApJL*, 946, L12

Baskin, A., & Laor, A. 2005, *MNRAS*, 358, 1043

Boquien, M., Burgarella, D., Roehlly, Y., et al. 2019, *Astronomy and Astrophysics*, 622, A103. <https://ui.adsabs.harvard.edu/abs/2019A&A...622A.103B>

Bradač, M., Huang, K.-H., Fontana, A., et al. 2019, *MNRAS*, 489, 99

Bradley, L., Sipocz, B., Robitaille, T., et al. 2016, *Astrophysics Source Code Library*, ascl:1609.011. <https://ui.adsabs.harvard.edu/abs/2016ascl.soft09011B>

Brammer, G. 2023, Zenodo, doi:10.5281/zenodo.7299500. <https://ui.adsabs.harvard.edu/abs/2022zndo...7299500B>

Bruzual, G., & Charlot, S. 2003, *Monthly Notices of the Royal Astronomical Society*, 344, 1000. <https://ui.adsabs.harvard.edu/abs/2003MNRAS.344.1000B>

Bushouse, H., Eisenhamer, J., Dencheva, N., et al. 2023, *JWST Calibration Pipeline*, v1.9.4, Zenodo, doi:10.5281/zenodo.7577320

Calzetti, D., Armus, L., Bohlin, R. C., et al. 2000, *The Astrophysical Journal*, 533, 682. <https://ui.adsabs.harvard.edu/abs/2000ApJ...533..682C>

Caputi, K. I., Deshmukh, S., Ashby, M. L. N., et al. 2017, *The Astrophysical Journal*, 849, 45. <https://ui.adsabs.harvard.edu/abs/2017ApJ...849...45C>

Caputi, K. I., Caminha, G. B., Fujimoto, S., et al. 2021, *The Astrophysical Journal*, 908, 146. <https://ui.adsabs.harvard.edu/abs/2021ApJ...908..146C>

Caputi, K. I., Rinaldi, P., Iani, E., et al. 2024, *The Astrophysical Journal*, 969, 159. <https://ui.adsabs.harvard.edu/abs/2024ApJ...969..159C>

Castellano, M., Napolitano, L., Fontana, A., et al. 2024, *ApJ*, 972, 143

Cataldi, E., Belfiore, F., Curti, M., et al. 2025, *A&A*, 703, A208

Chabrier, G. 2003, Publications of the Astronomical Society of the Pacific, 115, 763.  
<https://ui.adsabs.harvard.edu/abs/2003PASP..115..763C>

Chen, C.-H., Ho, L. C., Li, R., & Zhuang, M.-Y. 2025, ApJ, 983, 60

Cooper, R. A., Caputi, K. I., Iani, E., et al. 2025, ApJ, 994, 102

Cresci, G., Mannucci, F., Maiolino, R., et al. 2010, Nature, 467, 811

de Graaff, A., Rix, H.-W., Carniani, S., et al. 2024, A&A, 684, A87

de Graaff, A., Rix, H.-W., Naidu, R. P., et al. 2025, A&A, 701, A168

Dekel, A., Dutta Chowdhury, D., Lapiner, S., et al. 2025, arXiv e-prints, arXiv:2511.07578

D'Eugenio, F., Maiolino, R., Perna, M., et al. 2025a, arXiv e-prints, arXiv:2503.11752

D'Eugenio, F., Cameron, A. J., Scholtz, J., et al. 2025b, ApJS, 277, 4

Diego, J. M., Sun, F., Palencia, J. M., et al. 2025, A&A, 703, A207

Ebihara, S., Fujii, M. S., Saitoh, T. R., et al. 2026, arXiv e-prints, arXiv:2601.04344

Eldridge, J. J., Stanway, E. R., Xiao, L., et al. 2017, Publications of the Astronomical Society of Australia, 34, e058, aDS Bibcode: 2017PASA...34...58E.  
<https://ui.adsabs.harvard.edu/abs/2017PASA...34...58E>

Elmegreen, D. M., & Elmegreen, B. G. 2017, ApJL, 851, L44

Endsley, R., Stark, D. P., Whitler, L., et al. 2024, Monthly Notices of the Royal Astronomical Society, 533, 1111, publisher: OUP ADS Bibcode: 2024MNRAS.533.1111E.  
<https://ui.adsabs.harvard.edu/abs/2024MNRAS.533.1111E>

Fahrion, K., Lyubenova, M., van de Ven, G., et al. 2021, A&A, 650, A137

Ferland, G. J., Porter, R. L., van Hoof, P. A. M., et al. 2013, Revista Mexicana de Astronomia y Astrofisica, 49, 137. <https://ui.adsabs.harvard.edu/abs/2013RMxAA..49..137F>

Ferland, G. J., Chatzikos, M., Guzmn, F., et al. 2017, Revista Mexicana de Astronomia y Astrofisica, 53, 385.  
<https://ui.adsabs.harvard.edu/abs/2017RMxAA..53..385F>

Ferruit, P., Jakobsen, P., Giardino, G., et al. 2022, Astronomy and Astrophysics, 661, A81.  
<https://ui.adsabs.harvard.edu/abs/2022A&A...661A..81F>

Furtak, L. J., Zitrin, A., Plat, A., et al. 2023, The Astrophysical Journal, 952, 142.  
<https://ui.adsabs.harvard.edu/abs/2023ApJ...952..142F>

Furtak, L. J., Secunda, A. R., Greene, J. E., et al. 2025, A&A, 698, A227

Galliano, F., Madden, S. C., Jones, A. P., Wilson, C. D., & Bernard, J.-P. 2005, A&A, 434, 867

Gardner, J. P., Mather, J. C., Abbott, R., et al. 2023, Publications of the Astronomical Society of the Pacific, 135, 068001.  
<https://ui.adsabs.harvard.edu/abs/2023PASP..135f8001G>

Gledhill, R., Strait, V., Desprez, G., et al. 2024, ApJ, 973, 77

Greene, J. E., & Ho, L. C. 2005, ApJ, 630, 122

Greene, J. E., Strader, J., & Ho, L. C. 2020, Annual Review of Astronomy and Astrophysics, 58, 257. <https://ui.adsabs.harvard.edu/abs/2020ARA&A..58..257G>

Greene, J. E., Labbe, I., Goulding, A. D., et al. 2024, The Astrophysical Journal, 964, 39.  
<https://ui.adsabs.harvard.edu/abs/2024ApJ...964...39G>

Guseva, N. G., Papaderos, P., Meyer, H. T., Izotov, Y. I., & Fricke, K. J. 2009, A&A, 505, 63

Harikane, Y., Zhang, Y., Nakajima, K., et al. 2023, The Astrophysical Journal, 959, 39.  
<https://ui.adsabs.harvard.edu/abs/2023ApJ...959...39H>

Harris, C. R., Millman, K. J., van der Walt, S. J., et al. 2020, Nature, 585, 357.  
<https://ui.adsabs.harvard.edu/abs/2020Natur.585..357H>

Harshan, A., Bradač, M., Abraham, R., et al. 2024, MNRAS, 532, 1112

Heintz, K. E., De Cia, A., Thöne, C. C., et al. 2023a, A&A, 679, A91

Heintz, K. E., Brammer, G. B., Giménez-Arteaga, C., et al. 2023b, Nature Astronomy, 7, 1517

Hirashita, H., Hunt, L. K., & Ferrara, A. 2002, MNRAS, 330, L19

Hviding, R. E., de Graaff, A., Miller, T. B., et al. 2025, A&A, 702, A57

Iani, E., Caputi, K. I., Rinaldi, P., et al. 2024, The Astrophysical Journal, 963, 97, publisher: IOP ADS Bibcode: 2024ApJ...963...97I.  
<https://ui.adsabs.harvard.edu/abs/2024ApJ...963...97I>

Inayoshi, K., & Ho, L. C. 2025, arXiv e-prints, arXiv:2512.03130

Inayoshi, K., & Maiolino, R. 2025, ApJL, 980, L27

Inayoshi, K., Murase, K., & Kashiyama, K. 2025, arXiv e-prints, arXiv:2509.19422

Izotov, Y. I., Guseva, N. G., Fricke, K. J., Krügel, E., & Henkel, C. 2014, A&A, 570, A97

Izotov, Y. I., Thuan, T. X., & Guseva, N. G. 2024, MNRAS, 527, 3486

Ji, X., Maiolino, R., Übler, H., et al. 2025, MNRAS, 544, 3900

Karman, W., Caputi, K. I., Caminha, G. B., et al. 2017, *A&A*, 599, A28

Kocevski, D. D., Finkelstein, S. L., Barro, G., et al. 2025, *ApJ*, 986, 126

Kokorev, V., Caputi, K. I., Greene, J. E., et al. 2024, *The Astrophysical Journal*, 968, 38. <https://ui.adsabs.harvard.edu/abs/2024ApJ...968...38K>

Labbé, I., Greene, J. E., Bezanson, R., et al. 2025, *ApJ*, 978, 92

Laor, A. 2006, *ApJ*, 643, 112

Lau, R. M., Hankins, M. J., Kasliwal, M. M., et al. 2021, *ApJ*, 909, 113

Lebouteiller, V., Heap, S., Hubeny, I., & Kunth, D. 2013, *A&A*, 553, A16

Liu, H., Jiang, Y.-F., Quataert, E., Greene, J. E., & Ma, Y. 2025, *ApJ*, 994, 113

Lotz, J. M., Koekemoer, A., Coe, D., et al. 2017, *ApJ*, 837, 97

Magorrian, J., Tremaine, S., Richstone, D., et al. 1998, *The Astronomical Journal*, 115, 2285. <https://ui.adsabs.harvard.edu/abs/1998AJ....115.2285M>

Maiolino, R., Scholtz, J., Witstok, J., et al. 2024, *Nature*, 627, 59. <https://ui.adsabs.harvard.edu/abs/2024Natur.627...59M>

Maiolino, R., Uebler, H., D'Eugenio, F., et al. 2025a, arXiv e-prints, arXiv:2505.22567

Maiolino, R., Risaliti, G., Signorini, M., et al. 2025b, *MNRAS*, 538, 1921

Mármol-Queraltó, E., McLure, R. J., Cullen, F., et al. 2016, *MNRAS*, 460, 3587

Martínez-González, S., Wünsch, R., Tenorio-Tagle, G., et al. 2022, *ApJ*, 934, 51

Matsuoka, K., Nagao, T., Marconi, A., et al. 2018, *A&A*, 616, L4

Matthee, J., Naidu, R. P., Brammer, G., et al. 2024, *The Astrophysical Journal*, 963, 129. <https://ui.adsabs.harvard.edu/abs/2024ApJ...963..129M>

McLure, R. J., Dunlop, J. S., Cullen, F., et al. 2018, *MNRAS*, 476, 3991

Mignoli, M., Feltre, A., Bongiorno, A., et al. 2019, *A&A*, 626, A9

Morishita, T., Liu, Z., Stiavelli, M., et al. 2025, arXiv e-prints, arXiv:2507.10521

Mowla, L., Iyer, K., Asada, Y., et al. 2024, *Nature*, 636, 332

Naiman, J. P., Ramirez-Ruiz, E., Debuhr, J., & Ma, C.-P. 2015, *ApJ*, 803, 81

Nakajima, K., & Maiolino, R. 2022, *Monthly Notices of the Royal Astronomical Society*, 513, 5134. <https://ui.adsabs.harvard.edu/abs/2022MNRAS.513.5134N>

Navarro-Carrera, R., Rinaldi, P., Caputi, K. I., et al. 2024, *The Astrophysical Journal*, 961, 207, publisher: IOP ADS Bibcode: 2024ApJ...961..207N. <https://ui.adsabs.harvard.edu/abs/2024ApJ...961..207N>

Neumayer, N., Seth, A., & Böker, T. 2020, *A&A Rv*, 28, 4

Nikopoulos, G. P., Watson, D., Sneppen, A., et al. 2025, arXiv e-prints, arXiv:2510.06362

Onoue, M., Kashikawa, N., Matsuoka, Y., et al. 2019, *ApJ*, 880, 77

Osterbrock, D. E., & Ferland, G. J. 2006, *Astrophysics of gaseous nebulae and active galactic nuclei*. <https://ui.adsabs.harvard.edu/abs/2006agna.book.....O>

Östlin, G., Amram, P., Bergvall, N., et al. 2001, *A&A*, 374, 800

Pacucci, F., Nguyen, B., Carniani, S., Maiolino, R., & Fan, X. 2023, *The Astrophysical Journal*, 957, L3. <https://ui.adsabs.harvard.edu/abs/2023ApJ...957L...3P>

Partmann, C., Naab, T., Lahén, N., et al. 2025, *MNRAS*, 537, 956

Pérez-Montero, E., Contini, T., Lamareille, F., et al. 2013, *A&A*, 549, A25

Portegies Zwart, S. F., Baumgardt, H., Hut, P., Makino, J., & McMillan, S. L. W. 2004, *Nature*, 428, 724

Portegies Zwart, S. F., Baumgardt, H., McMillan, S. L. W., et al. 2006, *ApJ*, 641, 319

Postman, M., Coe, D., Benítez, N., et al. 2012, *ApJS*, 199, 25

Prieto-Jiménez, C., Álvarez-Márquez, J., Colina, L., et al. 2025, *A&A*, 701, A31

Prez-Gonzlez, P. G., Barro, G., Rieke, G. H., et al. 2024, *The Astrophysical Journal*, 968, 4. <https://ui.adsabs.harvard.edu/abs/2024ApJ...968....4P>

Reddy, N. A., Shapley, A. E., Sanders, R. L., et al. 2018, *The Astrophysical Journal*, 869, 92. <https://ui.adsabs.harvard.edu/abs/2018ApJ...869...92R>

Reddy, N. A., Shapley, A. E., Kriek, M., et al. 2020, *ApJ*, 902, 123

Reines, A. E., & Volonteri, M. 2015, *ApJ*, 813, 82

Rémy-Ruyer, A., Madden, S. C., Galliano, F., et al. 2013, *A&A*, 557, A95

Richard, J., Claeysse, A., Lagattuta, D., et al. 2021, *A&A*, 646, A83

Rinaldi, P., Caputi, K. I., Costantin, L., et al. 2023, *The Astrophysical Journal*, 952, 143, publisher: IOP ADS Bibcode: 2023ApJ...952..143R. <https://ui.adsabs.harvard.edu/abs/2023ApJ...952..143R>

Rinaldi, P., Navarro-Carrera, R., Caputi, K. I., et al. 2025a, *ApJ*, 981, 161

Rinaldi, P., Bonaventura, N., Rieke, G. H., et al. 2025b, *ApJ*, 992, 71

Ronayne, K., Papovich, C., Kirkpatrick, A., et al. 2025, arXiv e-prints, arXiv:2508.20177

Rusakov, V., Watson, D., Nikopoulos, G. P., et al. 2025, arXiv e-prints, arXiv:2503.16595

Rusta, E., Salvadori, S., Gelli, V., et al. 2025, ApJL, 989, L32

Sarmento, R., Scannapieco, E., & Pan, L. 2017, ApJ, 834, 23

Sarrouh, G. T. E., Asada, Y., Martis, N. S., et al. 2026, ApJS, 282, 3

Schaerer, D., Marques-Chaves, R., Barrufet, L., et al. 2022, A&A, 665, L4

Schwarz, G. 1978, The Annals of Statistics, Ann. Statist., 6, 461

Setton, D. J., Greene, J. E., Spilker, J. S., et al. 2025, ApJL, 991, L10

Shapley, A. E., Sanders, R. L., Reddy, N. A., Topping, M. W., & Brammer, G. B. 2023, ApJ, 954, 157

Shivaei, I., Reddy, N., Rieke, G., et al. 2020, ApJ, 899, 117

Stalevski, M., Ricci, C., Ueda, Y., et al. 2016, Monthly Notices of the Royal Astronomical Society, 458, 2288

Su, Z., Li, Z., & Li, Z. 2025, ApJ, 988, 68

Taylor, A. J., Kokorev, V., Kocevski, D. D., et al. 2025, ApJL, 989, L7

Taylor, M. 2022, 532, 3, conference Name: Astronomical Data Analysis Software and Systems XXX.  
<https://ui.adsabs.harvard.edu/abs/2022ASPC..532....3T>

team, T. p. d. 2024, pandas-dev/pandas: Pandas, Zenodo, doi:10.5281/zenodo.13819579.  
<https://zenodo.org/records/13819579>

Tenorio-Tagle, G., Wünsch, R., Silich, S., Muñoz-Tuñón, C., & Palouš, J. 2010, ApJ, 708, 1621

Theios, R. L., Steidel, C. C., Strom, A. L., et al. 2019, ApJ, 871, 128

Tripodi, R., Martis, N., Markov, V., et al. 2025, Nature Communications, 16, 9830

Troncoso, P., Maiolino, R., Sommariva, V., et al. 2014, A&A, 563, A58

Trussler, J. A. A., Conselice, C. J., Adams, N., et al. 2025, MNRAS, 537, 3662

Übler, H., Maiolino, R., Curtis-Lake, E., et al. 2023, Astronomy and Astrophysics, 677, A145. <https://ui.adsabs.harvard.edu/abs/2023A&A...677A.145U/abstract>

Vanzella, E., De Barros, S., Cupani, G., et al. 2016, ApJL, 821, L27

Vanzella, E., Caminha, G. B., Rosati, P., et al. 2021, A&A, 646, A57

Vanzella, E., Loiacono, F., Bergamini, P., et al. 2023, A&A, 678, A173

Yan, Z., Inayoshi, K., Chen, K., & Guo, J. 2025, arXiv e-prints, arXiv:2512.11050

Yang, H., Malhotra, S., Rhoads, J. E., & Wang, J. 2017, ApJ, 847, 38